Long-Term High-Resolution Gauge Adjusted Satellite Rainfall Product over India

Prashant Kumar[1], Atul K. Varma[1], Takuji Kubota[2], Moeka Yamaji[2],

Tomoko Tashima[2], Tomoaki Mega[3], and Tomoo Ushio[3]

1. Atmospheric and Oceanic Sciences Group, EPSA, Space Applications Centre, ISRO, India.

2. Earth Observation Research Center, Japan Aerospace Exploration Agency, Tsukuba, Japan.

3. Graduate School of Engineering, Osaka University, Suita, Japan.

ABSTRACT

This study aims to create a 21-year, high spatiotemporal resolution Global Satellite Mapping of Precipitation (GSMaP) rainfall product adjusted by rain gauge measurements over the Indian mainland. The targeted resolutions of the GSMaP are hourly and $0.1° \times 0.1°$. The National Oceanic and Atmospheric Administration (NOAA) Climate Prediction Center (CPC) daily gauge analysis $(0.5° \times 0.5°)$ and Indian Meteorological Department (IMD) daily gridded rainfall product $(0.25° \times 0.25°)$ were utilized to generate two long-term rainfall products, GSMaP_CPC and GSMaP_IMD rainfall, respectively. After preliminary verification of the GSMaP_CPC and GSMaP_IMD rainfalls with IMD gauges, these rainfall products are evaluated for the Indian Summer Monsoon (ISM) periods of 2000–2020 with comparisons of other merged rainfall products such as the Integrated Multi-satellitE Retrievals for Global Precipitation Measurement (IMERG). The results suggest GSMaP_IMD has a smaller root-mean-square difference (RMSD) and higher correlation than GSMaP_CPC, evaluated against independent rainfall products. In the three-hour mean analysis with spaceborne precipitation radar data, it is found that the value of RMSD decreases in GSMaP_IMD with respect to GSMaP_CPC throughout the day. The statistics against the hourly dense rain gauge network in Karnataka suggests that the GSMaP_IMD is more effective in capturing large spatiotemporal rainfall variation over India. Thus, validation results with the independent sources suggest that GSMaP_IMD rainfall generally improved over GSMaP_CPC rainfall. These improvements are significant in orographic regions with high rainfall amounts, mainly the western Ghats and northeastern parts of India.

Keywords: *Rainfall; gauges; satellite; validation; precipitation radar.*

1. Introduction

Precipitation is the primary source of fresh water globally and a key component of the global water budget (Kidd et al. 2021). The physical processes of precipitation occur on diverse spatiotemporal scales and drive its highly variable intermittency, intensity, areal extent, and duration. This large variability poses challenges to observations, specifically by spaceborne sensors (Adler et al. 2001; Ebert et al. 2007; Kirstetter et al. 2020; Varma and Liu 2006, 2010; Varma et

1

al. 2004). Further, converting satellite measurements into precipitation poses challenges due to large spatial heterogeneity, rain, no-rain, and rain type (e.g., convective, stratiform, warm, and orographic) classification, the indirect nature of measurements from thermal infrared (TIR) and high-frequency microwave (e.g., >85 GHz) passive instruments, the sensor resolution and sensitivity, and the retrieval algorithm (Kubota et al. 2007, 2009; Maggioni et al. 2016, 2022; Piyush et al. 2012; Varma 2018; You et al. 2022). Hence, satellite precipitation retrievals often suffer from poorly characterized and quantified sources of uncertainty, which currently limit their applications (Beck et al. 2017; Kumar and Varma 2017; Sun et al. 2018; Yamaji et al. 2021).

To overcome these issues partially, precipitation retrievals from active and passive microwave (PMW) sensors onboard Low Earth Orbiting (LEO) satellites (having higher accuracy but limited spatial and temporal resolution) are combined with infrared (IR) precipitation estimates from Geosynchronous Earth Orbiting (GEO) satellites. The merging takes advantage of their higher spatiotemporal resolution and lower latency (Joyce et al. 2004; Ushio et al. 2009; Kubota et al. 2020; Huffman et al. 2020). Further rain gauge observed rainfall is crucial to calibrate IR-MW retrieved precipitation products (Mega et al. 2019; Tashima et al. 2020). Although satellite precipitation estimates, adjusted by rain gauge data, were improved, but the spatial variability of precipitation is inadequate to characterize because of the sparse distribution of gauges. Earlier studies also showed that high-resolution precipitation products calibrated with daily gauge measurements are more accurate than those calibrated with monthly gauge measurements (Beck et al. 2019; Sharifi and Brocca 2022; Sharifi et al. 2019 and references therein).

The large spatiotemporal rainfall variations over India's mainland during the Indian Summer Monsoon (ISM) period make this region a unique testbed to access the quality of various global rainfall products (e.g., Brown 2006). Further, a large part of India's population depends on ISM rainfall data, which plays a vital role in its economy and agriculture. The localized heavy rainfall events in strong wind shear associated with monsoonal systems are often tilted (Sharma et al. 2022; Shige and Kummerow 2016) and also play a vital role that complicates rainfall estimation further. The study of ISM variability is also of interest to weather and climate modeling researchers who need precise long-term rainfall estimates. The large uncertainties are reported for various merged rainfall products, largely over western Ghats and the northeastern parts of India (Brown 2006; Kumar et al. 2021; Prakash et al. 2018; Shige et al. 2014).

This study examined a long-term (21-year) high spatiotemporal resolution Global Satellite Mapping of Precipitation (GSMaP) rainfall product developed for the Indian landmass using the rain gauges of the Indian Meteorological Department (IMD). The details of various rainfall data used in this study for developing and verifying new GSMaP rainfall products and the methodology to generate new GSMaP rainfall products are given in Section 2. The results are summarized in Section 3 and concluded in the last Section.

2. Data and Method

2.1. IMD Gauge Rainfall

This study used the dataset for IMD daily gridded rainfall over the Indian mainland (0.25° ×0.25°, Table 1) for 2000–2020 (Pai et al. 2014, 2015). To develop this rainfall product, Pai et al. (2014) utilized 6955 gauges in India with varying observing intervals, available from the National Data Centre, IMD, India. The IMD data for the last 24 hours (ending at 0830 Indian Standard Time (IST) [0300 UTC {Universal Time Coordinate}]) are used for multi-stage quality control of rain gauge observations before releasing the daily gridded rainfall dataset (Pai et al. 2014). In addition to the daily gridded rainfall dataset, station-measured rainfall was also utilized in this study for verification (Table 1).

2.2. JAXA GSMaP Rainfall

GSMaP is a precipitation product that uses combined data from the PMW sensors in low Earth orbit and IR radiometers in geostationary Earth orbit (Kubota et al. 2020; Table 1). The GSMaP_MVK product was also created, based on a Kalman filter model that refines the precipitation rate propagated and based on the cloud-moving vector derived from two successive IR images (Ushio et al. 2009). GSMaP was developed by the Japan Aerospace Exploration Agency (JAXA) for the Global Precipitation Measurement (GPM) mission as the standard Japanese GPM product. The product Version 03 (algorithm Version 6) data were used in this study. The horizontal resolution is $0.1° \times 0.1°$ on a lat/long grid, and the temporal resolution is one hour. The operating system of the JAXA GPM mission adjusts the GSMaP product with a three-day latency based on the NOAA/CPC unified gauge-based analysis of global daily precipitation (Kubota et al. 2020). The algorithm used an optimal estimation scheme, in which the solution is calculated by maximizing the probability density function defined in the system model (Mega et al. 2019). In this paper, the GSMaP product adjusted by the CPC rain gauges is referred to as "GSMaP_CPC" to distinguish it from the GSMaP product adjusted by the IMD rain gauges (Table 1).

2.3. Integrated Multi-satellitE Retrievals for GPM (IMERG) Final Rainfall

The IMERG rainfall product was developed as the standard US GPM product (Huffman et al. 2020) and is one of the products used for corrected rainfall data over the globe (Table 1). This rainfall product uses microwave sensor data and IR-based observations from all constellations of geosynchronous satellites. The monthly gauge precipitation data from Global Precipitation Climatology Centre (GPCC) rain gauges (Schneider et al. 2014) are utilized in the final IMERG product to correct for the bias of satellite retrievals over the land (Huffman et al. 2020). This gauge-adjusted rainfall product provides post-real-time rainfall estimates after four months of data retrieval. This rainfall product is available at the 0.1° spatial and half-hourly temporal resolutions.

2.4. TRMM/PR and GPM/DPR rainfall

The independent reference data for validation was from spaceborne precipitation radar products derived from precipitation radar aboard the Tropical Rainfall Measuring Mission (TRMM/PR, Kummerow et al. 1998; Kozu et al. 2001) and Dual-frequency precipitation radar onboard the GPM Core Observatory (GPM/DPR, Hou et al. 2014; Skofronick-Jackson et al. 2017). We used precipitation rate data at the estimated surface level from the TRMM/PR and GPM/DPR (Ku-band precipitation radar algorithm) Version 06A product (Seto et al. 2021) for June to September (JJAS) of 2000-2020. In Version 06A, better continuity of the TRMM/PR and GPM/DPR data was realized by reconsidering calibration coefficients and applying common precipitation estimation algorithms. The orbit-basis rainfall data from level-2 products are re-gridded for 0.1° spatial resolution, the same as the GSMaP resolution used for comparisons. It should be noted that the TRMM/PR and GPM/DPR rainfall data are not directly input to the GSMaP algorithm. However, physical precipitation models based on the TRMM/PR and GPM/DPR observations are incorporated into the radiative transfer model calculation for generating look-up tables (Kubota et al. 2020).

2.5. NCMRWF merged satellite gauge rainfall

The National Centre for Medium-Range Weather Forecasting (NCMRWF) Merged Satellite Gauge (NMSG, Table 1) rainfall product developed by Mitra et al. (2013) is a merged daily rainfall product with 0.25° spatial resolution using background rainfall from real-time GPM (earlier TRMM multisatellite precipitation analysis [TMPA]) and IMD gridded rainfall over India. The authors used successive correction methods to produce the analysis on a uniform latitude-longitude grid. The authors found that the NMSG daily rainfall has additional information due to the inclusion of IMD gauge observations. In the absence of TMPA, Reddy et al. (2019) used the GPM-based GSMaP-NRT rainfall as a background for generating merged rainfall data.

2.6. KSNDMC Dense Gauge Network

The Indian state of Karnataka is located between 11°50 N and 18°50 N and 74° E and 78°50 E and is enclosed by a dense rain gauge network that is a unique testbed for verifying rainfall products (Kumar et al. 2021). This state has a tableland region, coastal plains, and mountain slopes in the western part of the Deccan Peninsula of India. The Karnataka State Natural Disaster Monitoring Centre (KSNDMC) deployed gauges whose data were utilized in this study to validate daily and hourly rainfall products. This study used data from the dense rain gauge network of the KSNDMC (6502 stations in 2018 with an average rain gauge density of 5800 stations during JJAS of 2016–2020) during ISM 2016–2020. The rain gauge sensor in this network is a tipping bucket with low tolerance made of polycarbonate or industrial standard metal (Kumar et al. 2021). The instrument's precision is 1 % rainfall intensity up to 50 mm day^{-1} and 2 % rainfall intensity of 50–100 mm day^{-1}. The original time resolution of

the observations was every 15 min using a tipping count method (0.2/0.5 mm per tip) with an operating range up to 600 mm hr^{-1}, but in this study, hourly and daily (defined as rainfall observed from the last day 0830 IST to the current day 0830 IST) were used for verification purposes.

2.7. Methodology

Recently, Kumar et al. (2021) demonstrated the importance of the gauge density and adjustment (or merging) technique for generating more trustworthy merged rainfall products for wider applications. This study was prompted by the need to improve the current gauge-adjusted daily rainfall prepared by an objective analysis (e.g., Cressman) over India. The authors showed that the maximum likelihood estimation (MLE) method based merged rainfall provide the optimal solution over an objective analysis method. Moreover, the current merged rainfall products over India are at coarser spatial (0.25° × 0.25°) and temporal (24-hour) resolution (e.g., NMSG rain). These concerns have encouraged the improvement of the merged rainfall products over India using an IMD gridded gauge-based rainfall product.

To achieve these objectives, identical experiments were conducted to adjust GSMaP_MVK rainfall using NOAA CPC rainfall analysis and IMD gridded rainfall for 2000–2020 based upon the method of Mega et al. (2019). The NOAA CPC and IMD gridded rainfall adjusted GSMaP rainfall products are GSMaP_CPC and GSMaP_IMD, respectively. This way, we could take advantage of the IMD gridded rainfall data generated by many gauges than the GSMaP_CPC rainfall product calibrated by NOAA CPC gauge analysis. The following steps were implemented to calibrate GSMaP_MVK rainfall using IMD gridded rain data: (1) First, due to a mismatch in spatial resolution, the IMD gridded rainfall was linearly interpolated at NOAA CPC spatial resolution (0.5° × 0.5°) from its original resolution (0.25° × 0.25°) over India. (2) In the next step, the MLE method was executed to update hourly GSMaP rainfall at a finer spatial resolution (0.1° × 0.1°) using daily gridded gauge analysis at a coarser 0.5° resolution from March 1, 2000 to December 31, 2020. Thus, the GSMaP hourly data with the 0.1° × 0.1° resolution are adjusted using the data of daily rain gauges with 0.5° × 0.5° resolution. The details of the adjustment of GSMaP rainfall using NOAA CPC analysis are given in Mega et al. (2019).

The various statistical methods (Wilks, 2006) were computed to validate the gauge-adjusted GSMaP rain against observations (e.g., gauges, satellite). The mean error (bias), the root-mean-square difference (RMSD), and the correlation coefficient were estimated for different rainfall products. Bias is an error that is used to find how gauge-adjusted rain deviated from observations and is defined as

$Bias = \frac{1}{N} \sum_{i=1}^{N} (G_i - O_i)$

where N is the number of samples; O and G are observed and gauge-adjusted GSMaP rainfall, respectively. Positive (negative) bias values indicate that estimates are overestimated (underestimated). RMSD measures the average error

5

magnitude and gives greater weight to the larger errors.

$$RMSD = \sqrt{\left(\frac{1}{N}\right) \sum_{i=1}^{N} (G_i - O_i)^2}$$

The correlation coefficient shows the relationship between Observation and gauge-adjusted rain products and measures the degree of linear association between the gauge-adjusted rainfall and observations.

Correlation Coefficient $(r) = \dfrac{\left[(\sum_{i=1}^{N} (O_i -_i)(G_i -_i) \right]}{\sqrt{\sum_{i=1}^{N}(O_i -_i)^2} \sqrt{\sum_{i=1}^{N}(G_i -_i)^2}}$, **Range: -1 to +1**

Here, $_i$ is the average of actual values, and $_i$ is the average of gauge-adjusted rainfall. Furthermore, various forecast accuracy scores were also computed using a contingency table (Bhomia et al. 2019). The Probability of Detection (POD), False Alarm Ratio (FAR), and Critical Success Index (CSI) present the ability of the gauge-adjusted rain products for different rainfall thresholds.

3. Results and Discussions

3.1. Verification of GSMaP rainfall against IMD gauges

Figure 1 shows the spatial distribution of the mean JJAS daily rainfall from IMD gridded rainfall, IMERG Final, GSMaP_CPC, and GSMaP_IMD for 2000–2020. The figure shows that the IMERG Final (Fig. 1b), GSMaP_CPC (Fig. 1c), and GSMaP_IMD (Fig. 1d) rainfall can capture low rainfall values over northwestern India, the rain-shadow region of the southern peninsula, and northern India when verified against IMD gridded rainfall (Fig. 1a). The IMERG Final and GSMaP_CPC rainfall capture high rainfall over western Ghats to some extent, but miss the spatial distribution of high rainfall over northeast India and foothills of the Himalaya. GSMaP_IMD rainfall (Fig. 1d) most closely replicates the high rainfall over these regions, showing the successful adjustment of the GSMaP rainfall with IMD gauges.

Similar to figure 1, the spatial distribution of the mean JJAS 2000–2020 daily rainfall from IMD gauges (gridded data), IMERG Final, GSMaP_CPC, and GSMaP_IMD rain products for the 36 heterogeneous meteorological zones shown in Figure 2. The IMERG Final (Fig. 2b) underestimated rainfall in the western Ghats regions. The distribution of rainfall is closer to IMD gauges (Fig. 2a) in GSMaP_IMD rain (Fig. 2d) than in GSMaP_CPC rainfall (Fig. 2c). These results reconfirm that the adjustment of IR-MW rain data using daily gauges is more accurate than data calibrated using monthly gauges. Overestimates were noted over northern India in a few rain regions. The figure shows larger uncertainties over northeast India when compared with IMD gridded gauge rainfall (Fig. 2a). The high rainfall over Sikkim, West Bengal, Assam, and Arunachal Pradesh was missing from IMERG Final and GSMaP_CPC data. Overestimates were noted over the Meghalaya, Tripura, and Assam states

in IMERG Final rain (Fig. 2b). The precise values of satellite rainfall retrieval over the northeast part of India are still problematical, and gauge-based adjustments are required for further application. The GSMaP_IMD rain can capture these large variations over this region after adjusting with IMD gauges (Fig. 2d). Overall, average rainfall values in different meteorological zones suggested adjustments to GSMaP_IMD data produce more accurate data.

Further, IMERG Final, GSMaP_CPC, and GSMaP_IMD daily rainfall are also compared with IMD gridded rainfall ($0.25° \times 0.25°$) and IMD stations rainfall for JJAS 2000–2020. The statistics in Figure 3(d, e, f) are based on the average of 2475 IMD stations per day during JJAS 2000–2020. The RMSD (bias) is around 14.7 (0.2) mm day^{-1} and 16.6 (0.3) mm day^{-1} when IMERG Final rainfall is compared with IMD gridded (Fig. 3a) and stations rainfall (Fig. 3d), respectively. The correlations are 0.61 and 0.59, contrasting with IMD gridded and IMD stations' rainfall, respectively. Similar to IMERG Final rainfall, GSMaP_CPC rainfall is closer to IMD gridded rainfall and presented a larger error when compared with IMD rainfall. The RMSD (bias) is 13.5 (-0.8) mm day^{-1} and 16.3 (-0.7) mm day^{-1} when compared with IMD gridded (Fig. 3b) and stations rainfall (Fig. 3e). The value of correlation changes from 0.60 (against IMD gridded rain) to 0.56 (against IMD stations rain). Results show that GSMaP_IMD has fewer errors in RMSD (bias) of 6.7 (-0.3) mm day^{-1} against IMD gridded rain (Fig. 3c) than IMD stations' rain (Fig. 3f). The smaller error in IMD gridded rain data at $0.25° \times 0.25°$ suggests that the GSMaP_IMD is closer to observations that are utilized to adjust the GSMaP_MVK rain at coarser resolution ($0.5° \times 0.5°$). RMSD (13.4 mm day^{-1}) and bias (-0.4 mm day^{-1}) are seen in GSMaP_IMD and are slightly larger when compared with IMD stations rain (Fig. 3f). This presents the large heterogeneity of rainfall within a grid. It suggests the need for a rainfall product with high spatial resolution. RMSD (bias) decreased from 16.3 (-0.7) mm day^{-1} in GSMaP_CPC rain (Fig. 3e) to 13.4 (-0.4) mm day^{-1} in GSMaP_IMD rain (Fig. 3f) compared to IMD stations rainfall. The correlation improved from 0.56 for GSMaP_CPC rain to 0.73 for GSMaP_IMD rain.

Figure 4 (similar to Figure 5 in Kubota et al. 2007) shows the cumulative rainfall using daily rainfall during JJAS 2000–2020, comparing the IMERG Final, GSMaP_CPC, and GSMaP_IMD to IMD gridded rain. The figure shows that the GSMaP_IMD rain is closer to IMD gridded rainfall ($0.25° \times 0.25°$) than IMERG Final and GSMaP_CPC rain products. The largest deviation can be seen in GSMaP_CPC rain. The probability distribution analysis (figure not shown) suggests that the IMERG Final, GSMaP_CPC, and GSMaP_IMD rain overestimate weak rainfall intensities. This overestimation is the maximum for IMERG Final rain. All rainfall products underestimate rainfall intensity, with the largest underestimation for IMERG Final product for middle to larger rainfall intensities. The GSMaP_IMD rain is slightly closer to IMD rain for all ranges than IMERG Final and GSMaP_CPC rain.

Figure 5 shows the spatial distribution of POD, FAR, and CSI for IMERG Final,

GSMaP_CPC, and GSMaP_IMD rainfall for a 0.5 mm day^{-1} rainfall threshold with IMD gridded rainfall as reference. The values of POD are higher than 0.7 in IMERG Final and GSMaP_CPC rain in most regions, except rain-shadow regions in the southern Indian peninsula and north and northwest India. Slightly larger values of POD are noted in GSMaP_CPC rain (Fig. 5b) over the western Ghats and northeastern and central India than in IMERG Final rain (Fig. 5a). However, IMERG Final shows larger POD over the rain-shadow region in the summer monsoon period. The value of POD is a maximum for GSMaP_IMD rain (Fig. 5c), which shows the importance of adjustment using IMD gauges. The smaller values of POD over Ladakh (situated in eastern J&K, India) are largely due to the sparse distribution of IMD gauges. The spatial distributions of FAR for IMERG Final, GSMaP_CPC, and GSMaP_IMD are shown in Figure 5(d, e, f). It shows larger FAR values over north and northwestern India, northeast India, and rain-shadow regions of southern peninsula India in IMERG Final (Fig. 5d) and GSMaP_CPC (Fig. 5e) rain. Generally, the value of FAR is the minimum for GSMaP_IMD rain (Fig. 5f). Similar to POD and FAR, CSI values show similar spatial distributions. The maximum values of CSI are achieved over central India. GSMaP_CPC (Fig. 5h) shows larger CSI over orographic regions, largely western Ghats and northeast India. Only GSMaP_IMD can capture IMD gauge observed rainfall over northern India satisfactorily. The spatial distributions of POD, FAR, and CSI are considerably less at high rainfall thresholds (15.5 mm day^{-1}), suggesting that there are large mismatches in precisely estimating the magnitude of larger rainfall in GSMaP_CPC and IMERG Final rain (figure not shown). These results suggest that the gauge adjustments are crucial for IMERG Final and GSMaP_CPC rain to estimate large spatial variations over India.

3.2. Comparison of GSMaP rainfall against independent rainfall products

After the preliminary verification of GSMaP_CPC and GSMaP_IMD derived rainfall against IMD gauges, the GSMaP_CPC and GSMaP_IMD rainfall products were validated using TRMM/PR and GPM/DPR products as independent satellite datasets. In order to compared with TRMM/PR and GPM/DPR, the GSMaP_CPC and GPM_IMD data are extracted along with the TRMM/PR and GPM/DPR orbits in the target domain, as shown in Fig. 1. Figure 6 shows the comparison of RMSD and correlation between GSMaP_CPC and GSMaP_IMD in a diurnal cycle. It was found that the value of RMSD (Fig. 6a) decreased in GSMaP_IMD compared with GSMaP_CPC throughout the day. The mean RMSD values of GSMaP_CPC and GSMaP_IMD were 1.03 mm hour^{-1} and 0.95 mm hour^{-1}, respectively. This result indicates that adjusting the satellite-based GSMaP rainfall with a localized gauge dataset can improve the GSMaP quantitative accuracy by approximately 10 %, more effectively than using the global gauge dataset of NOAA CPC. In addition, the spatial correlation coefficient (Fig. 6b) of GSMaP_IMD was better than GSMaP_CPC even though the IMD adjustment worsened the results in 15–21 LT slightly; the mean values of the spatial correlation coefficient for GSMaP_CPC and GSMaP_IMD

were 0.236 and 0.241, respectively. This result indicates that the spatial pattern of rainfall can be detected more closely by IMD adjustment than NOAA CPC adjustment. However, it should be noted that the spatial correlation can vary depending on the limitation of observation sampling of TRMM/PR and GPM/DPR overpasses.

3.3. Comparison of GSMaP rainfall against NMSG gridded rainfall

The density plots of GSMaP_CPC and GSMaP_IMD daily rainfall against NMSG merged daily rainfall (Table 1) during JJAS 2017-2020 are shown in Figure 7. The NMSG rainfall product is available at 0.25° spatial resolution, requiring interpolation of GSMaP rainfall at the same resolution. The total number of collocations is 2.2 million. The value of RMSD (bias) improved from 13.9 (-0.2) mm day^{-1} for GSMaP_CPC to 12.5 (-0.0) mm day^{-1} in GSMaP_IMD rainfall. The correlation coefficient improved from 0.61 in GSMaP_CPC to 0.71 in GSMaP_IMD against the NMSG merged rainfall product. The verification with NMSG rainfall was also extended for monthly statistics. The values of RMSD and correlation for different months during ISM suggested that RMSD values are larger in July and August (peak monsoon months) and least in September. Generally, the correlation improved in GSMaP_IMD over GSMaP_CPC rainfall for all months (figure not shown).

3.4. Comparison of GSMaP rainfall against KSNDMC dense gauge network

The dense rain gauge network of KSNDMC was also utilized to validate daily rainfall from IMERG Final, GSMaP_CPC, and GSMaP_IMD during JJAS 2016–2020. There was an average of 5800 gauges in Karnataka during this period. These gauges are well distributed over Karnataka, covering rainfall ranging from extremely high over the western Ghats to low in the rain-shadow regions. The density plot of IMERG and GSMaP rainfalls against KSNDMC gauges observed rainfall is shown in Figure 8. The value of RMSD (bias) decreased from 15.8 (-2.9) mm day^{-1} in GSMaP_CPC (Fig. 8b) to 14.0 (-0.8) mm day^{-1} in GSMaP_IMD rainfall (Fig. 8c). Slightly fewer errors were found in the IMERG Final rain (Fig. 8a), with RMSD (bias) values of 15.0 (-0.4) mm day^{-1}, than GSMaP_CPC rain. The correlation coefficient also improved from 0.52 in IMERG Final and 0.4 in GSMaP_CPC to 0.56 in GSMaP_IMD rainfall. These results suggested that the GSMaP rainfall data improved considerably after IMD gauge adjustment in the state of Karnataka with independent gauges.

Further, these results are also extended for hourly rainfall verifications over Karnataka for JJAS 2018 only (Fig. 9). In general, the bias is less in IMERG Final and GSMaP_IMD rain than GSMaP_CPC rain (Fig. 9a). These results reconfirmed that the GSMaP_IMD rainfall has less RMSD (Fig. 9b) and a higher correlation (Fig. 9c) than GSMaP_CPC rainfall. It is important to note that for this period (JJAS 2018), the performance of the GSMaP_CPC was better than IMERG Final rain, having less RMSD and higher correlation

9

values. These improvements were recognized for different synoptic hours. These statistics suggest that the GSMaP_IMD is more skilful in capturing the large spatiotemporal variation of rainfall over India and can be extended to diverse applications.

To examine the spatial characteristics of IMERG Final, GSMaP_CPC, and GSMaP_IMD rain, KSNDMC gauges were divided as being in four meteorological zones—**Malnad** (the western Ghats), **Coastal** (a region of heavy rainfall), **NIK,** and **SIK** (rain-shadow region). The rainfall values are maximum in the coastal and Malnad regions and are considerably lower in the NIK and SIK rain-shadow regions. Further details about these regions are available in Kumar et al. (2021). Figure 10 compares IMERG Final, GSMaP_CPC, and GSMaP_IMD rain to the KSNDMC dense gauge network for Malnad (Figs. 10(a, c, e)) and coastal (Figs. 10(b, d, f)) regions, mostly in high rainfall regions. The values of RMSD (bias) changed from 26.3 (-9.9) mm day^{-1} in GSMaP_CPC to 23.1 (-4.3) mm day^{-1} in GSMaP_IMD rain in Malnad regions during the summer monsoons 2016–2020. The RMSD (bias) errors are 24.3 (-4.1) mm day^{-1} in IMERG Final rain and have less bias than GSMaP_CPC rain. The correlation values improved from 0.29 in GSMaP_CPC and 0.41 in IMERG Final rain to 0.45 in GSMaP_IMD rain for the Malnad region. The errors are slightly larger in the coastal regions, mainly for GSMaP_CPC rain. The RMSD (bias) value is 25.7 (-6.0) mm day^{-1} in IMERG Final, 31.2 (-16.1) mm day^{-1} in GSMaP_CPC rain and 24.6 (-3.1) mm day^{-1} in GSMaP_IMD products for JJAS 2016–2020. A large negative bias (-16.1 mm day^{-1}) in GSMaP_CPC indicates that it needs further modifications to capture high rainfall over western Ghat regions that decrease after IMD gauge adjustment. In general, correlation values improved for both Malnad and the coastal regions. These results suggest that gauge corrections are crucial over orographic and coastal regions where IR-MW retrieved rainfall is more inaccurate. Similar to the verification of IMERG Final, GSMaP_CPC, and GSMaP_IMD rain in high rainfall regions, these rain products were also compared over rain-shadow regions where rainfall is much less during the summer monsoon season (Fig. 11). Marginal changes are observed in error statistics for both SIK (Figs. 11(a, c, e)) and NIK (Figs. 11(b, d, f)) regions between GSMaP_CPC and GSMaP_IMD rain. In general, IMERG Final rain has larger errors over these regions. Moreover, bias values are negligible over these regions, except in IMERG Final rain (1.2 mm day^{-1}) over NIK regions. The correlation is the maximum for IMERG Final rain over these regions. Overall, these results suggest that the adjustment of satellite retrievals with gauges is most crucial in mountainous regions.

4. Conclusions

This study aims to adjust the GSMaP rainfall using IMD gauges over the Indian mainland and compare the performance of the GSMaP_IMD rainfall product to the operational GSMaP_CPC rainfall product adjusted by NOAA/CPC rainfall. The daily rain gauges adjust the GSMaP hourly data with a 0.1° × 0.1° resolution. In the preliminary verification, GSMaP_IMD rainfall was close to IMD

gridded rainfall and IMD stations rainfall. These verifications were performed at different spatial and temporal scales for JJAS 2000–2020 and evaluated by various statistical scores. In the long-term verifications of GSMaP rainfalls against IMD gauges, the improvements were significant over orographic regions with high rainfall amounts, mainly western Ghats and northeast India. The IMERG Final and GSMaP_CPC rainfall captured high rainfall over western Ghats but missed spatial distribution of high rainfall over the northeastern part of India and the foothills of the Himalayas. However, the GSMaP_IMD rainfall that most closely replicates the high rainfalls over these regions demonstrated the successful adjustment of the GSMaP rainfall with IMD gauge data.

Moreover, various independent sources of rainfall from gauges (the KSNDMC dense gauge network), spaceborne precipitation radar retrievals (TRMM/PR and GPM/DPR), and merged rainfall products (IMERG Final and NMSG) were utilized for rigorous verification at different temporal scales. In the three-hour mean analysis with TRMM/PR and the GPM/DPR data, it was found that the value of RMSD decreased in GSMaP_IMD with respect to GSMaP_CPC throughout the day. The statistics against the KSNDMC hourly gauges suggested that the GSMaP_IMD was more effective in capturing large spatiotemporal rainfall variation over India. Thus, validation results with the independent sources suggested that GSMaP_IMD rainfall generally improved over GSMaP_CPC rainfall. These large improvements in GSMaP_IMD rainfall are largely due to quality control gauge observations from IMD, India. The magnitude of improvements was the maximum over orographic regions compared with independent gauge observations.

Acknowledgments

References

Adler, R. F., Kidd, C., Petty, G., Morissey, M., & Goodman, H. M. (2001). Intercomparison of global precipitation products: The third Precipitation Intercomparison Project (PIP-3). *Bulletin of the American Meteorological Society*, *82*(7), 1377–1396.

Beck, H. E., Vergopolan, N., Pan, M., Levizzani, V., Van Dijk, A. I., Weedon, G. P., Brocca, L., Pappenberger, F., Huffman, G. J., & Wood, E. F. (2017). Global-scale evaluation of 22 precipitation datasets using gauge observations and hydrological modeling. *Hydrology and Earth System Sciences*, *21*(12), 6201–6217.

Beck, H. E., Pan, M., Roy, T., Weedon, G. P., Pappenberger, F., Van Dijk, A. I.,... & Wood, E. F. (2019). Daily evaluation of 26 precipitation datasets using Stage-IV gauge-radar data for the CONUS. *Hydrology and Earth System Sciences*, *23*(1), 207–224.

Bhomia, S., Kumar, P., and Kishtawal, C. M. (2019). Evaluation of the weather research and forecasting model forecasts for Indian summer monsoon rainfall of 2014 using ground-based observations. *Asia-Pacific Journal of Atmospheric Sciences*, *55*(4), 617–628.

Brown, J. E. (2006). An analysis of the performance of hybrid infrared and microwave satellite precipitation algorithms over India and adjacent regions. *Remote Sensing of Environment*, *101*(1), 63–81.

Ebert, E. E., Janowiak, J. E., & Kidd, C. (2007). Comparison of near-real-time precipitation estimates from satellite observations and numerical models. *Bulletin of the American Meteorological Society*, *88*(1), 47–64.

Hou, A. Y., Kakar, R. K., Neeck, S., Azarbarzin, A. A., Kummerow, C. D., Kojima, M., Oki, R., Nakamura, K., & Iguchi, T. (2014) The Global Precipitation Measurement Mission. *Bull. Am. Meteorol. Soc., 95*, 701–722.

Huffman, G. J., Bolvin, D. T., Braithwaite, D., Hsu, K. L., Joyce, R. J., Kidd, C.,... & Xie, P. (2020). Integrated multi-satellite retrievals for the global precipitation measurement (GPM) mission (IMERG). In *Satellite precipitation measurement* (343–353). Springer, Cham.

Joyce, R. J., Janowiak, J. E., Arkin, P. A., & Xie, P. (2004). CMORPH: A method that produces global precipitation estimates from passive microwave and infrared data at high spatial and temporal resolution. *Journal of hydrometeorology*, *5*(3), 487–503.

Kidd, C., Huffman, G., Maggioni, V., Chambon, P., & Oki, R. (2021). The Global Satellite Precipitation Constellation: current status and future requirements. *Bulletin of the American Meteorological Society*, *102*(10), E1844-E1861.

Kirstetter, P. E., Petersen, W. A., Kummerow, C. D., & Wolff, D. B. (2020). Integrated Multi-satellite Evaluation for the Global Precipitation Measurement: Impact of Precipitation Types on Spaceborne Precipitation Estimation. In *Satellite Precipitation Measurement* (583–608). Springer, Cham.

Kubota, T., Shige, S., Hashizume, H., Aonashi, K., Takahashi, N., Seto, S.,... & Okamoto, K. I. (2007). Global precipitation map using satellite-borne microwave radiometers by the GSMaP project: Production and validation. *IEEE Transactions on Geoscience and Remote Sensing*, *45*(7), 2259–2275.

Kubota, T., Ushio, T., Shige, S., Kida, S., Kachi, M., & Okamoto, K. I. (2009). Verification of high-resolution satellite-based rainfall estimates around Japan using a gauge-calibrated ground-radar dataset. *Journal of the Meteorological Society of Japan. Ser. II*, *87*, 203-222.

Kubota, T., Aonashi, K., Ushio, T., Shige, S., Takayabu, Y. N., Kachi, M.,... & Oki, R. (2020). Global Satellite Mapping of Precipitation (GSMaP) products in the GPM era. In *Satellite precipitation measurement* (355–373). Springer, Cham.

Kumar, P., & Varma, A. K. (2017). Assimilation of INSAT-3D hydro-estimator method retrieved rainfall for short-range weather prediction. *Quarterly Journal of the Royal Meteorological Society*, *143*(702), 384–394.

Kumar, P., Gairola, R., Kubota, T., & Kishtawal, C. (2021). Hybrid assimilation of satellite rainfall product with high density gauge network to improve daily estimation: A case of Karnataka, India. *Journal of the Meteorological Society of Japan. Ser. II.* https://doi.org/10.2151/jmsj.2021-037

Kozu, T., Reddy, K. K., Mori, S., Thurai, M., Ong, J. T., Rao, D. N., & Shimomai, T. (2006). Seasonal and diurnal variations of raindrop size distribution in Asian monsoon region. *J. Meteorol. Soc. Japan*, *84A*, 195–209.

Kummerow, C., Barnes, W., Kozu, T., Shiue, J., & Simpson, J. (1998). The Tropical Rainfall Measuring Mission (TRMM) sensor package. *J. Atmos. Ocean. Technol., 15*, 809–817.

Maggioni, V., Meyers, P. C., & Robinson, M. D. (2016). A review of merged high-resolution satellite precipitation product accuracy during the Tropical Rainfall Measuring Mission (TRMM) era. *Journal of Hydrometeorology*, *17*(4), 1101–1117.

Maggioni, V., Massari, C., & Kidd, C. (2022). Errors and uncertainties associated with quasiglobal satellite precipitation products. In *Precipitation Science* (377–390). Elsevier.

Mega, T., Ushio, T., Takahiro, M., Kubota, T., Kachi, M., & Oki, R. (2018). Gauge-adjusted global satellite mapping of precipitation. *IEEE Transactions on Geoscience and Remote Sensing*, *57*(4), 1928–1935.

Mitra, A. K., Momin, I. M., Rajagopal, E. N., Basu, S., Rajeevan, M. N., & Krishnamurti, T. N. (2013). Gridded daily Indian monsoon rainfall for 14 seasons: Merged TRMM and IMD gauge analyzed values. *Journal of Earth System Science*, *122*(5), 1173–1182.

Pai, D. S., Rajeevan, M., Sreejith, O. P., Mukhopadhyay, B., & Satbha, N. S. (2014). Development of a new high spatial resolution (0.25× 0.25) long period (1901–2010) daily gridded rainfall data set over India and its comparison with current data sets over the region. *Mausam*, *65*(1), 1–18.

Pai, D. S., Sridhar, L., Badwaik, M. R., & Rajeevan, M. (2015). Analysis of the daily rainfall events over India using a new long period (1901–2010) high resolution (0.25× 0.25) gridded rainfall data set. *Climate dynamics*, *45*(3), 755–776.

Piyush, D. N., Varma, A. K., Pal, P. K., & Liu, G. (2012). An analysis of rainfall

measurements over different spatio-temporal scales and potential implications for uncertainty in satellite data validation. *Journal of the Meteorological Society of Japan. Ser. II*, *90*(4), 439–448.

Prakash, S., Mitra, A. K., AghaKouchak, A., Liu, Z., Norouzi, H., & Pai, D. S. (2018). A preliminary assessment of GPM-based multi-satellite precipitation estimates over a monsoon dominated region. *Journal of Hydrology*, *556*, 865–876.

Reddy, M. V., Mitra, A. K., Momin, I. M., Mitra, A. K., & Pai, D. S. (2019). Evaluation and inter-comparison of high-resolution multi-satellite rainfall products over India for the southwest monsoon period. *International Journal of Remote Sensing*, *40*(12), 4577–4603.

Schneider, U., Becker, A., Finger, P., Meyer-Christoffer, A., Ziese, M., & Rudolf, B. (2014). GPCC's new land surface precipitation climatology based on quality-controlled in situ data and its role in quantifying the global water cycle. *Theoretical and Applied Climatology*, *115*(1), 15–40.

Seto, S., Iguchi, T., Meneghini, R., Awaka, J., Kubota, T., Masaki, T., & Takahashi, N. (2021). The precipitation rate retrieval algorithms for the GPM Dual-frequency Precipitation Radar. *Journal of the Meteorological Society of Japan. Ser. II*, *99*(2), 205–237.

Sharifi, E., Saghafian, B., & Steinacker, R. (2019). Downscaling satellite precipitation estimates with multiple linear regression, artificial neural networks, and spline interpolation techniques. *Journal of Geophysical Research: Atmospheres*, *124*(2), 789–805.

Sharifi, E., & Brocca, L. (2022). Monitoring precipitation from space: progress, challenges, and opportunities. In *Precipitation Science* (239–255). Elsevier.

Sharma, N., Varma, A. K., & Liu, G. (2022). Percentage occurrence of global tilted deep convective clouds under strong vertical wind shear. *Advances in Space Research*, *69*(6), 2433–2442.

Shige, S., Yamamoto, M. K., & Taniguchi, A. (2014). Improvement of TMI rain retrieval over the Indian subcontinent. *Remote sensing of the terrestrial water cycle*, *206*, 27-42.

Shige, S., & Kummerow, C. D. (2016). Precipitation-top heights of heavy orographic rainfall in the Asian monsoon region. *Journal of the Atmospheric Sciences*, *73*(8), 3009–3024.

Skofronick-Jackson, G., Petersen, W. A., Berg, W., Kidd, C., Stocker, E. F., Kirschbaum, D. B., Kakar, R., Braun, S. A., Huffman, G. J., Iguchi, T., Kirstetter, P. E., Kummerow, C., Meneghini, R., Oki, R., Olson, W. S., Takayabu, Y. N., Furukawa, K., & Wilheit, T. (2017). The Global Precipitation Measurement (GPM) mission for science and society. *Bull. Am. Meteorol. Soc., 98,* 1679–1695.

Sun, Q., Miao, C., Duan, Q., Ashouri, H., Sorooshian, S., & Hsu, K. L. (2018). A review of global precipitation data sets: Data sources, estimation, and inter-comparisons. *Reviews of Geophysics*, *56*(1), 79–107.

Tashima, T., Kubota, T., Mega, T., Ushio, T., & Oki, R. (2020). Precipitation extremes monitoring using the near-real-time GSMaP product. *IEEE Journal of Selected Topics in Applied Earth Observations and Remote Sensing*, *13*, 5640–5651.

Ushio, T., Sasashige, K., Kubota, T., Shige, S., Okamoto, K. I., Aonashi, K., Inoue, T., Takahashi, N., Iguchi, T., Kachi, M., Oki, R., Morimoto, T., & Kawasaki, Z. I. (2009). A Kalman filter approach to the Global Satellite Mapping of Precipitation (GSMaP) from combined passive microwave and infrared radiometric data. *Journal of the Meteorological Society of Japan. Ser. II*, *87*, 137–151.

Varma, A. K., Liu, G., & Noh, Y. J. (2004). Subpixel-scale variability of rainfall and its application to mitigate the beam-filling problem. *Journal of Geophysical Research: Atmospheres*, *109*(D18).

Varma, A. K., & Liu, G. (2006). Small-scale horizontal rain-rate variability observed by satellite. *Monthly weather review*, *134*(10), 2722–2733.

Varma, A. K., & Liu, G. (2010). On classifying rain types using satellite microwave observations. *Journal of Geophysical Research: Atmospheres*, *115*(D7).

Varma, A. K. (2018). Measurement of Precipitation from Satellite Radiometers (Visible, Infrared, and Microwave): Physical Basis, Methods, and Limitations. In *Remote Sensing of Aerosols, Clouds, and Precipitation* (223–248). Elsevier.

Wilks, D. S., 2006: Statistical Methods in the Atmospheric Sciences. 2nd ed. Academic Press, 627 pp.

Yamaji, M., Kubota, T., & Yamamoto, M. K. (2021). An Approach to Reliability Characterization of GSMaP Near-Real-Time Precipitation Product. *Journal of the Meteorological Society of Japan. Ser. II*. https://doi.org/10.2151/jmsj.2021-033.

You, Y., Wang, N. Y., Kubota, T., Aonashi, K., Shige, S., Kachi, M., Kummerow, C., Randel, D., Ferraro, R., Braun, S., & Takayabu, Y. (2020). Comparison of TRMM Microwave Imager rainfall datasets from NASA and JAXA. *Journal of Hydrometeorology*, *21*(3), 377–397.

Table 1: Details of selected rainfall products.

@ >p(- 8) * >p(- 8) * >p(- 8) * >p(- 8) * >p(- 8) * @ **Product name** & **Spatial resolution** & **Temporal resolution**

(in hour) & **Coverage** & **Sensors**

KSNDMC Dense Gauge Network

& - & Hourly during JJAS 2018 and daily during JJAS 2016-2020 & Over Karnataka only & Rain gauges

IMD Gridded Gauge Rainfall

& 0.25° ×0.25° & Daily during 2000-2020 & Indian landmass & Rain gauges

IMERG Final Rainfall

& 0.1° × 0.1° & Half-hourly during 2000-2020 & Global domain of 60° S to 60° N & IR, MW & GPCC monthly gauge analysis

NCMRWF Merged Satellite Gauge Rainfall

& 0.25° ×0.25° & Daily during 2017-2020 & 50°E-110°E

30° S-40° N & GPM rainfall + IMD gauges

GSMaP_MVK

& 0.1° × 0.1° & Hourly during 2000-2020 & Global domain of 60° S to 60° N & IR & MW

GSMaP_CPC

& 0.1° × 0.1° & Hourly during 2000-2020 & Global domain of 60° S to 60° N & IR, MW & NOAA CPC daily Gauge analysis

GSMaP_IMD

& 0.1° × 0.1° & Hourly during 2000-2020 & Global domain of 60° S to 60° N & IR, MW, NOAA CPC daily Gauge analysis and IMD gauges over India
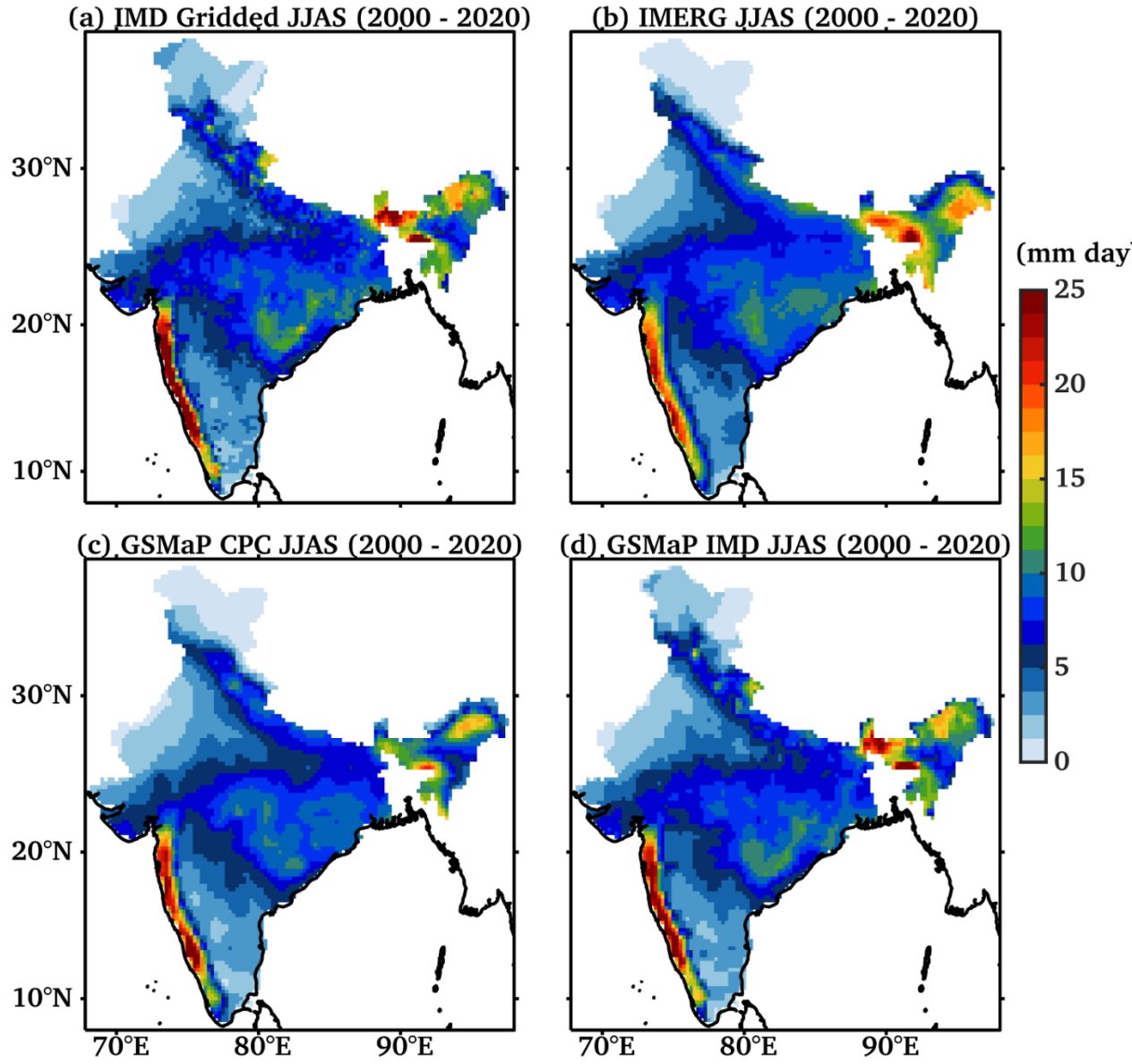
Figure 1. Spatial distribution of mean daily rainfall from (a) IMD gridded rain, (b) IMERG Final rain, (c) GSMaP_CPC rain, and (d) GSMaP_IMD rain during the Indian summer monsoons (JJAS; June to September months) 2000–2020.
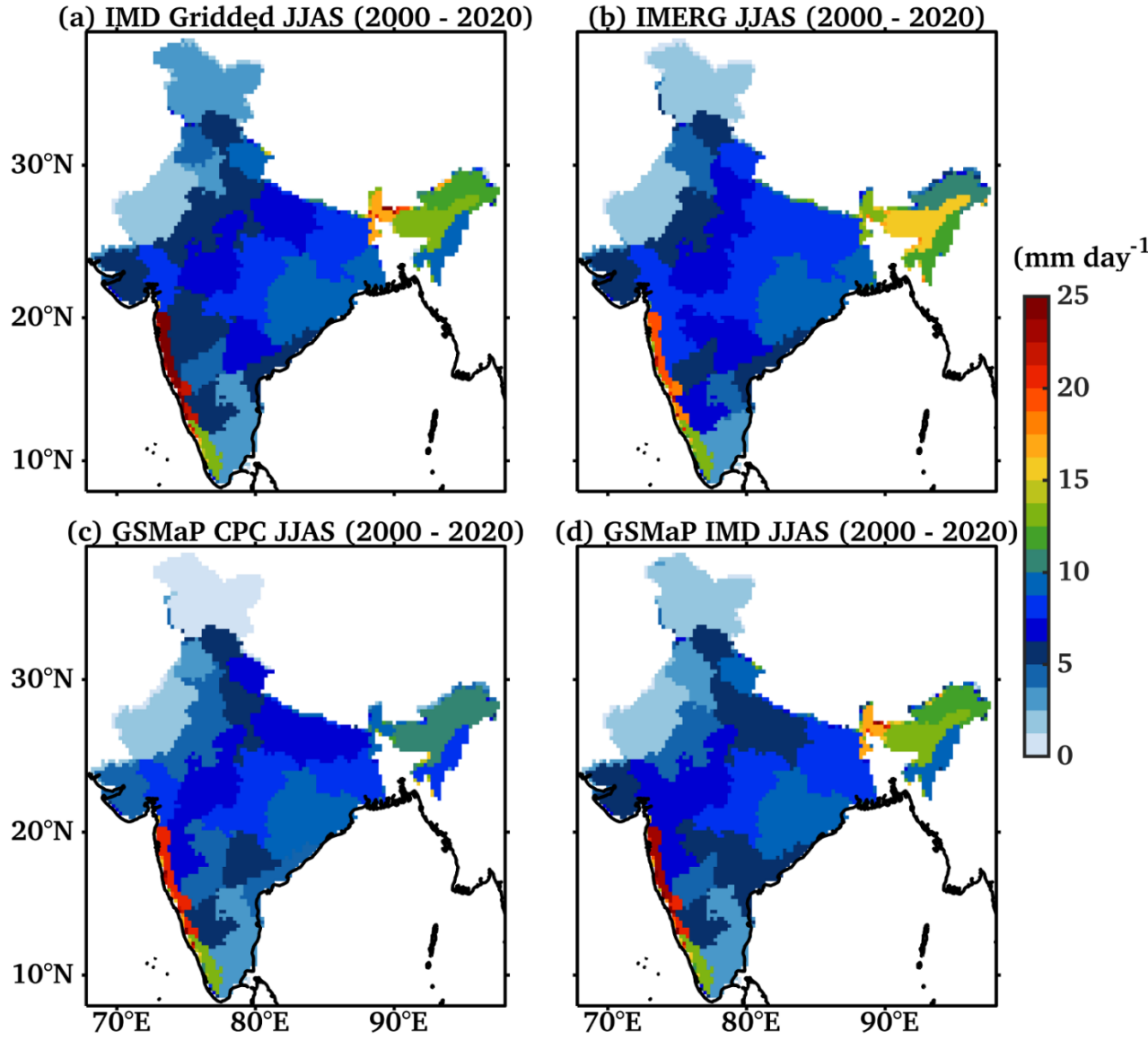
(a) IMD Gridded JJAS (2000 - 2020)

(b) IMERG JJAS (2000 - 2020)

(c) GSMaP CPC JJAS (2000 - 2020)

(d) GSMaP IMD JJAS (2000 - 2020)

Figure 2. Same as Figure 1 but for different meteorological zones of India.
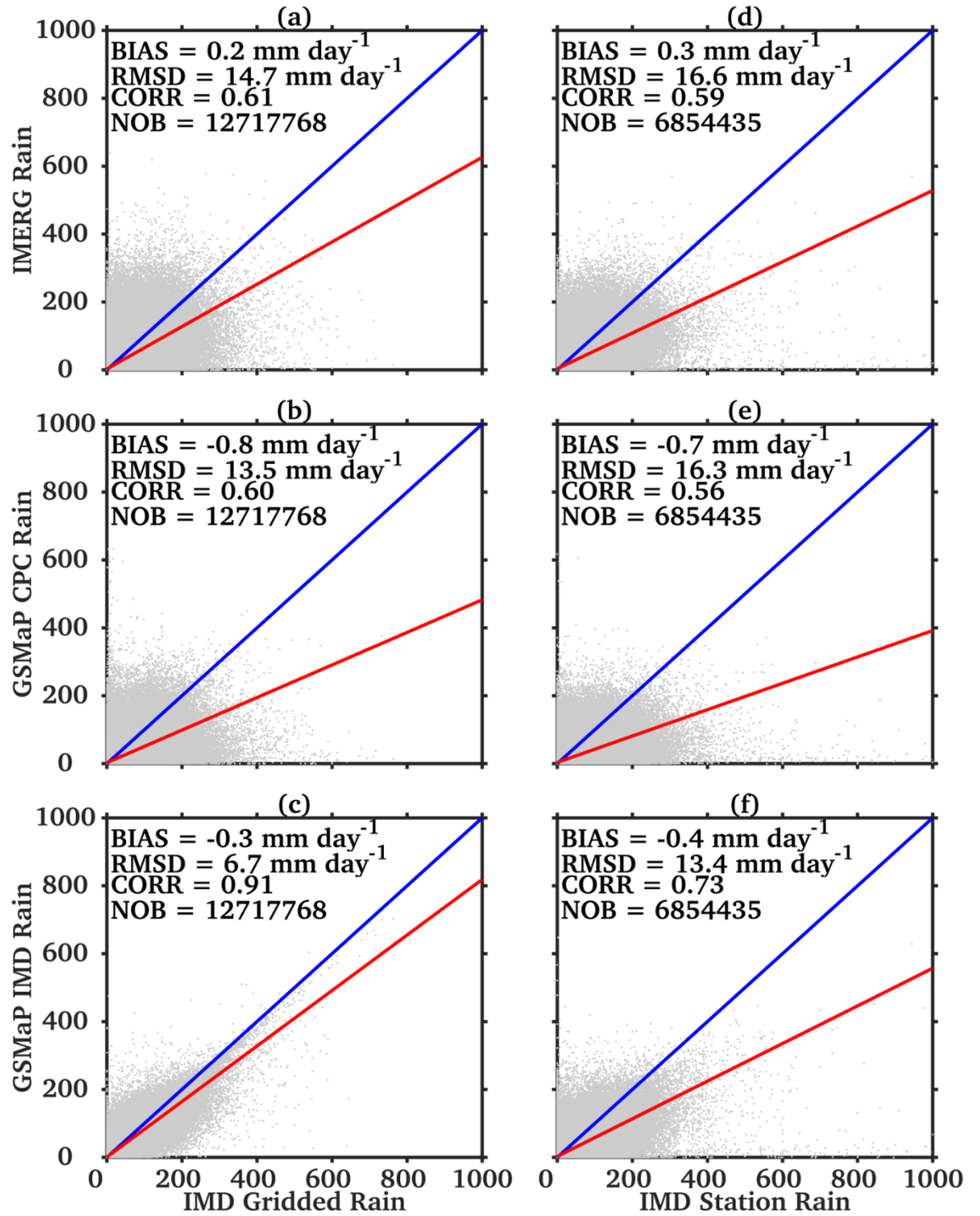
Figure 3. Comparison of IMERG Final, GSMaP_CPC, and GSMaP_IMD rainfall vs. IMD gridded and stations rainfall during JJAS 2000–2020. Scatter plots (a) IMERG, (b) GSMaP_CPC, (c) GSMaP_IMD daily rainfall vs. IMD gridded rainfall (at 0.25˚ x 0.25˚), and (d) IMERG, (e) GSMaP_CPC, (f) GSMaP_IMD daily rainfall vs. IMD station daily rainfall.
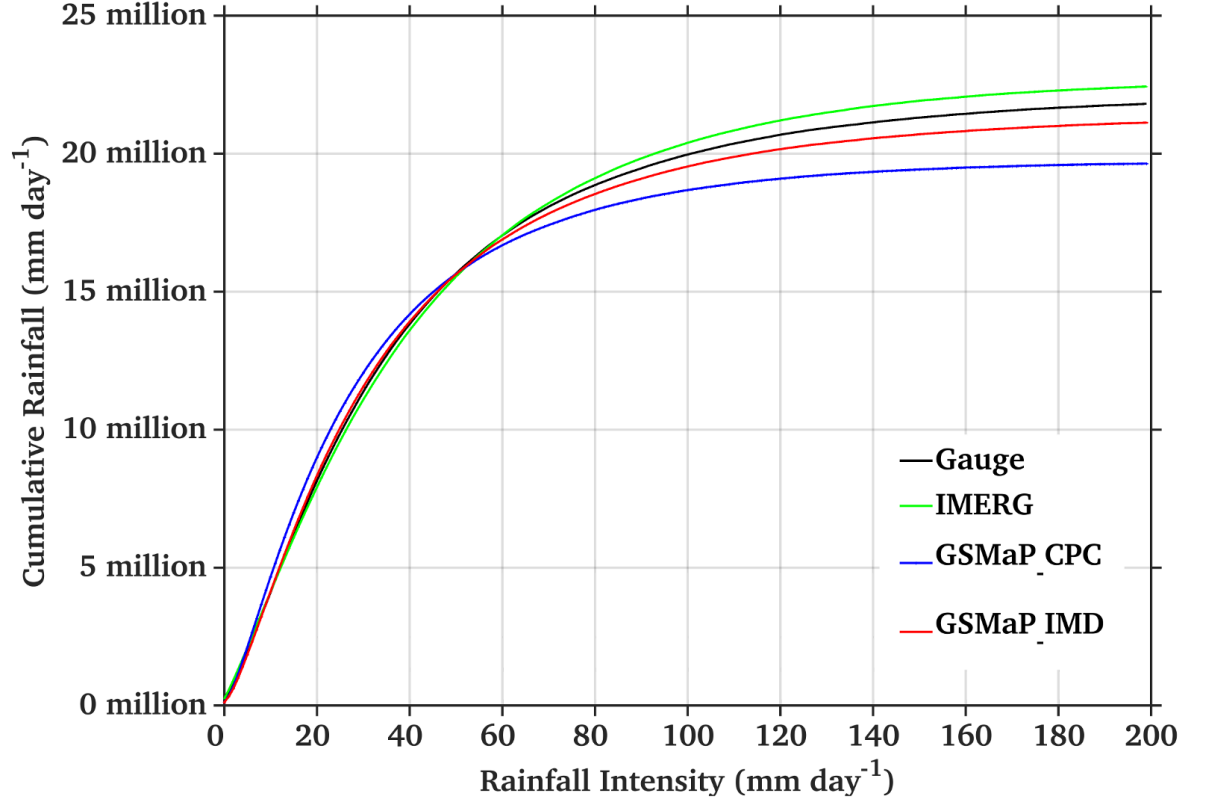
Figure 4. Cumulative rainfall over Indian landmass during ISM 2000–2020. The width of the bin is 1 mm day^{-1}. This analysis is done for IMD gridded rainfall (at 0.25˚ x 0.25˚).
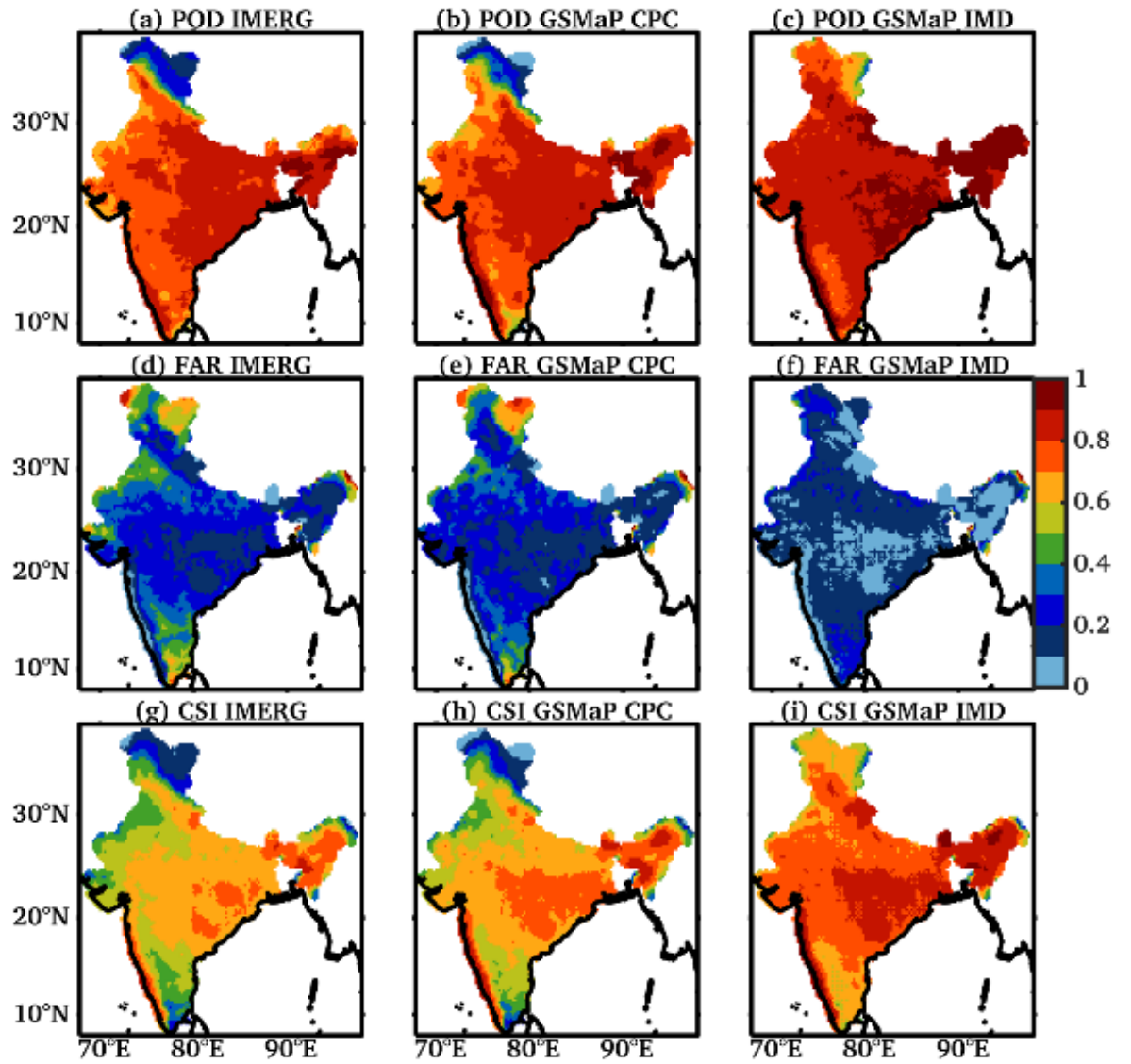
Figure 5. Statistical scores of IMERG (left), GSMaP_CPC (middle), and GSMaP_IMD (right) with IMD gridded rainfall with 0.5 mm/day threshold during JJAS 2000–2020.
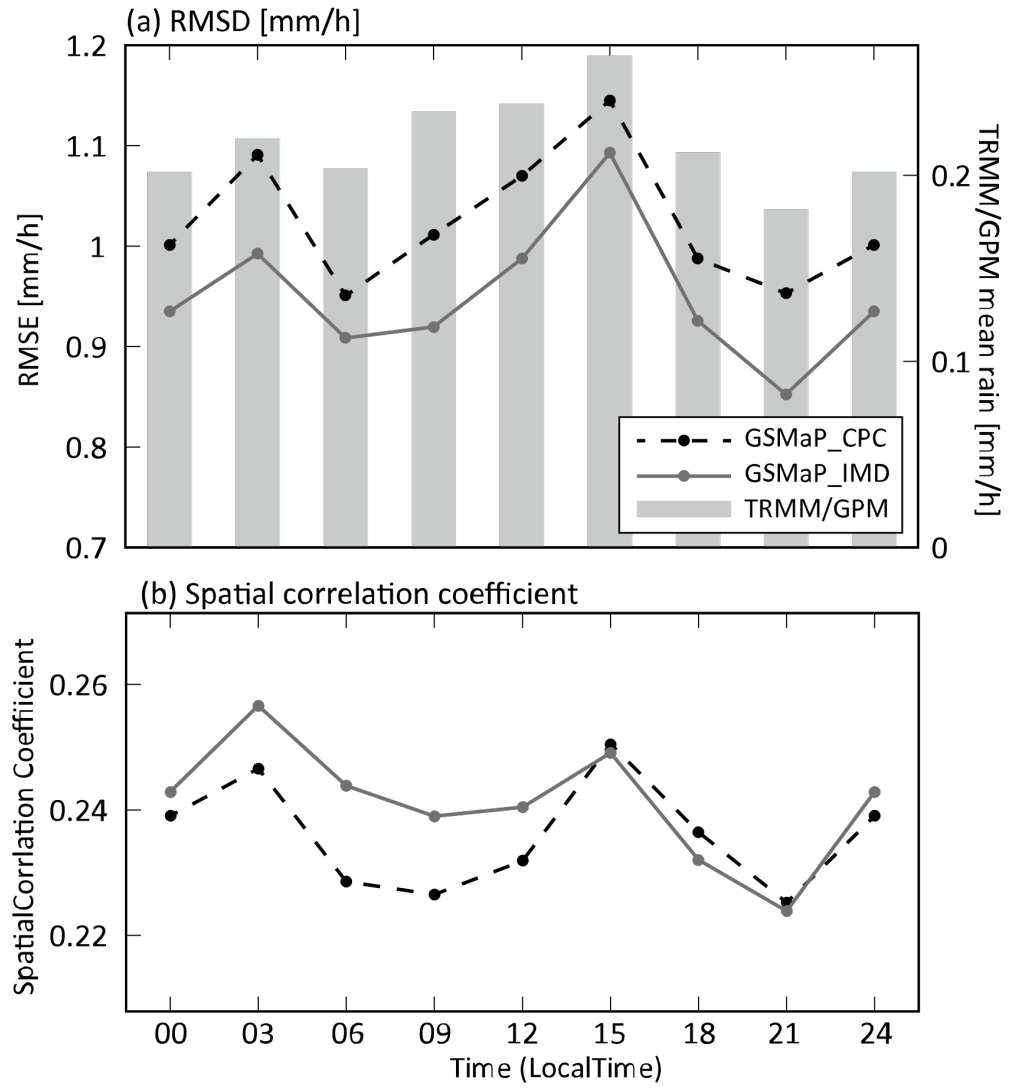
Figure 6. Three-hour mean values of (a) RMSD for GSMaP_CPC (dashed black line) and GSMaP_IMD (solid gray line) with mean rainfall from TRMM/GPM (gray boxes with right vertical axis), and (b) spatial correlation coefficient for GSMaP_CPC (dashed black line) and GSMaP_IMD (solid gray line).
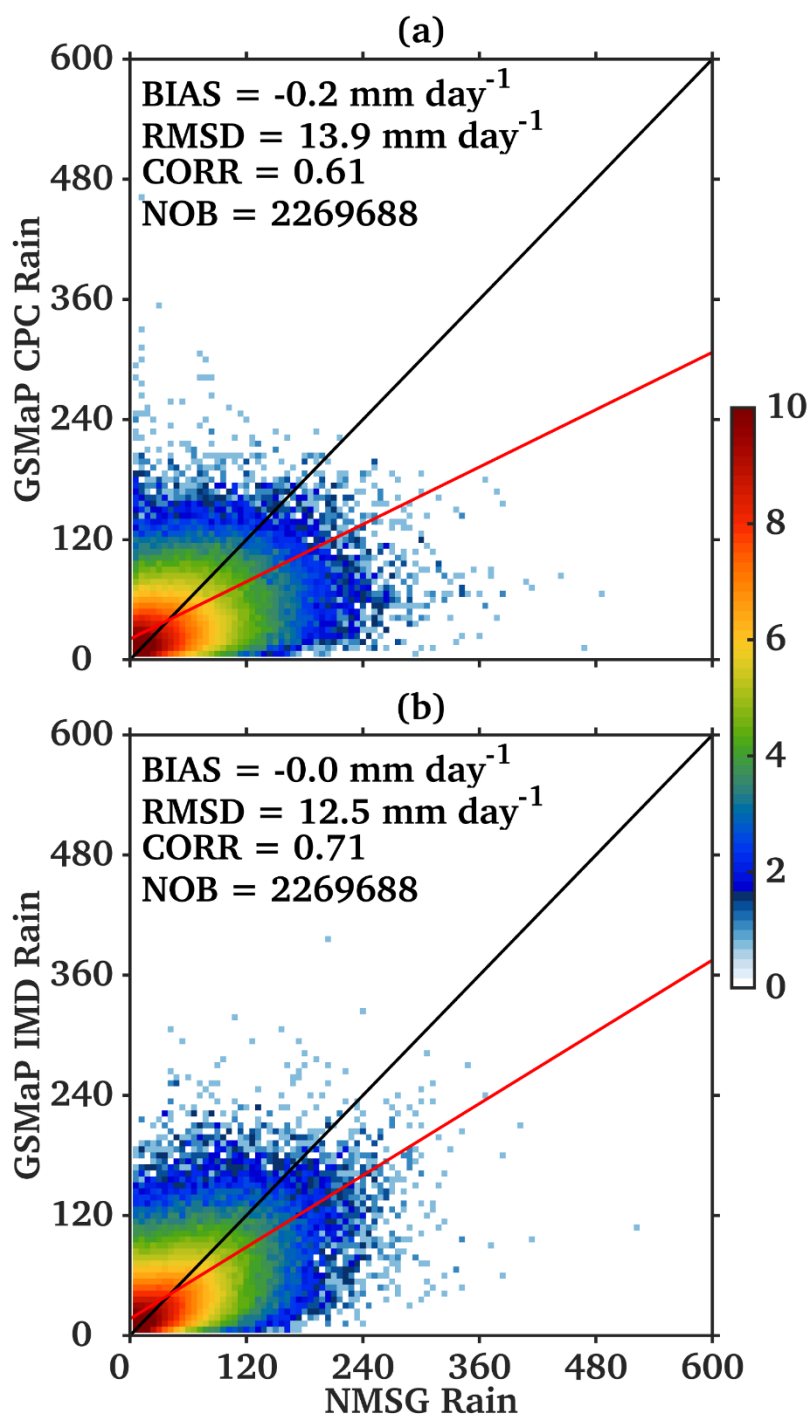
(a)

BIAS = -0.2 mm day^{-1}
RMSD = 13.9 mm day^{-1}
CORR = 0.61
NOB = 2269688

GSMaP CPC Rain

(b)

BIAS = -0.0 mm day^{-1}
RMSD = 12.5 mm day^{-1}
CORR = 0.71
NOB = 2269688

GSMaP IMD Rain

NMSG Rain

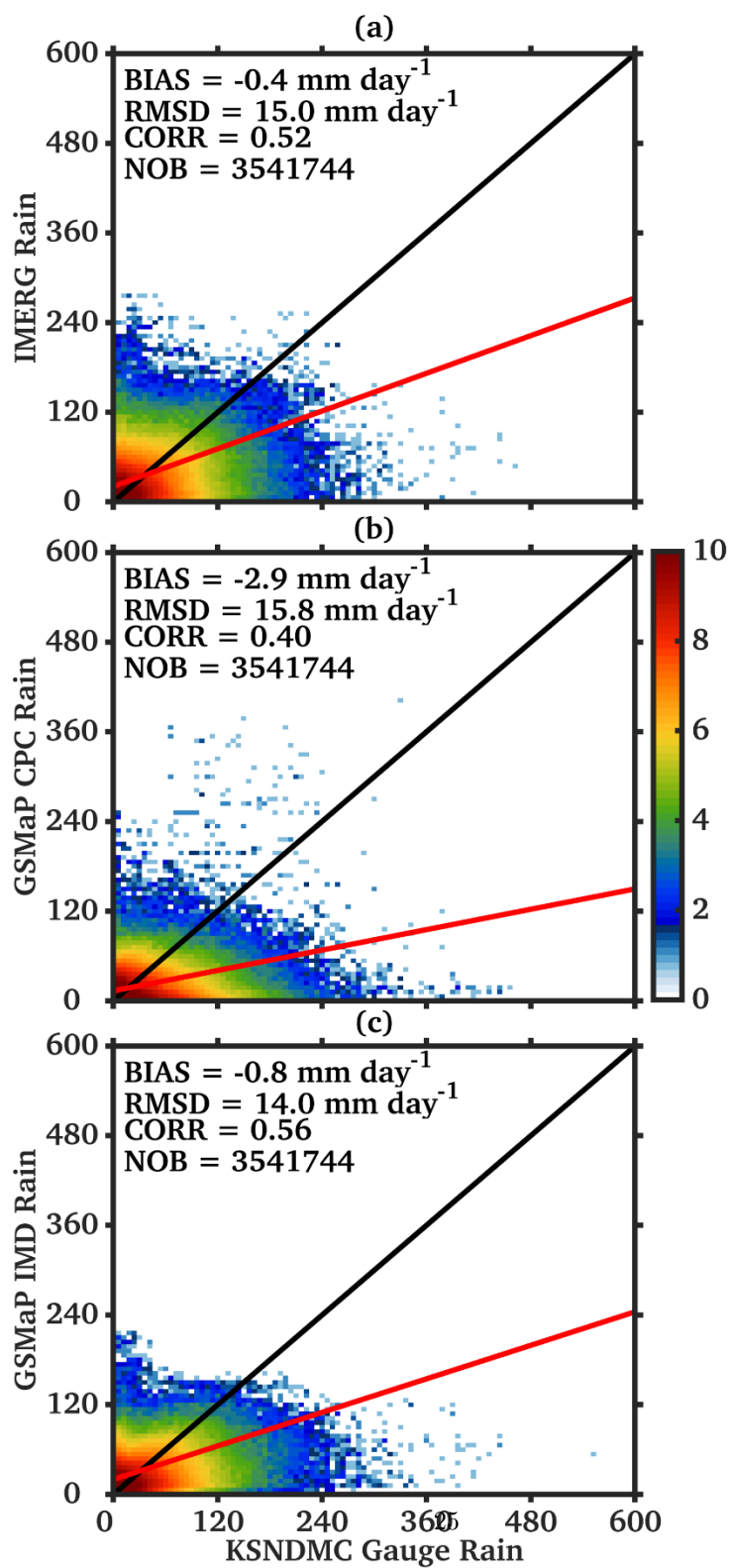Figure 7. Comparison of daily (a) GSMaP_CPC and (b) GSMaP_IMD rainfall vs. NMSG rainfall for JJAS 2017–2020.

(a)

BIAS = -0.4 mm day^{-1}
RMSD = 15.0 mm day^{-1}
CORR = 0.52
NOB = 3541744

(b)

BIAS = -2.9 mm day^{-1}
RMSD = 15.8 mm day^{-1}
CORR = 0.40
NOB = 3541744

(c)

BIAS = -0.8 mm day^{-1}
RMSD = 14.0 mm day^{-1}
CORR = 0.56
NOB = 3541744

IMERG Rain

GSMaP CPC Rain

GSMaP IMD Rain

KSNDMC Gauge Rain

25

Figure 8. Comparison of (a) IMERG Final, (b) GSMaP_CPC, and (c) GSMaP_IMD daily rainfall vs. KSNDMC dense rain gauge network for JJAS 2016–2020.
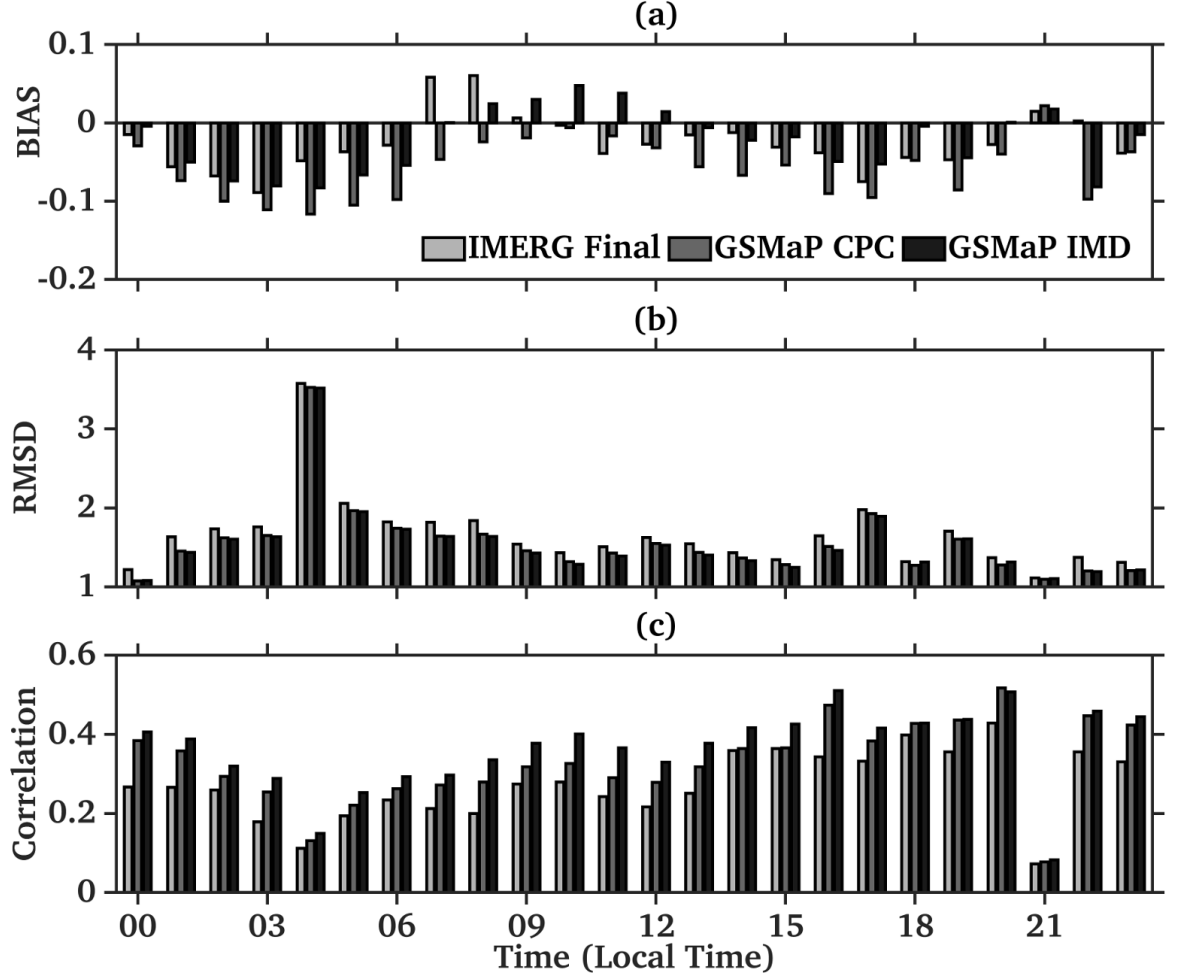
Figure 9. The hourly (a) Bias, (b) RMSD, and (c) Correlation statistics of IMERG Final, GSMaP_CPC, and GSMaP_IMD rainfall vs. KSNDMC hourly gauges during JJAS 2018.
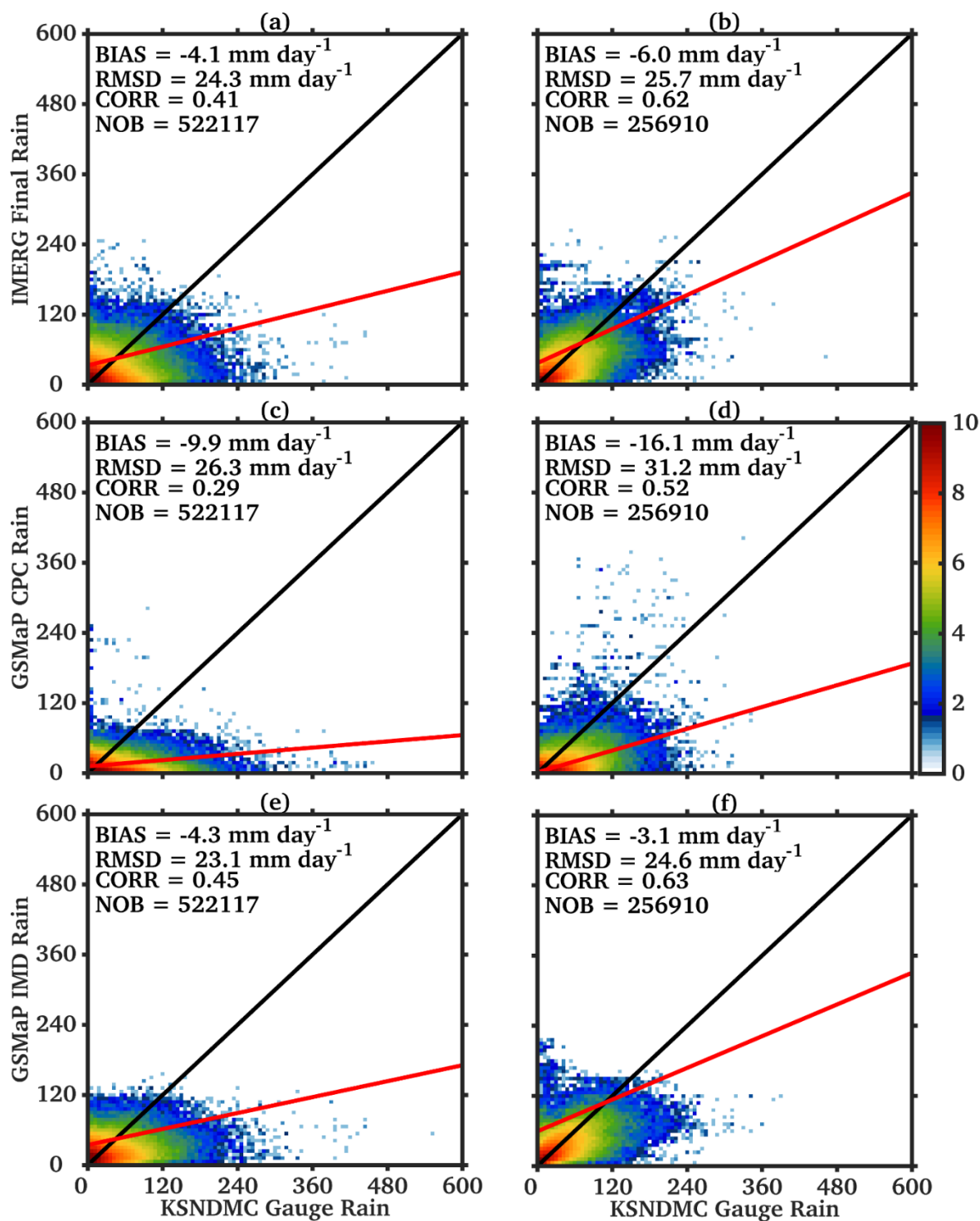
Figure 10. Comparison of IMERG Final, GSMaP_CPC, and GSMaP_IMD rain vs. KSNDMC dense rain gauge network for (a, c, e) Malnad and (b, d, f) coastal regions for JJAS 2016–2020.
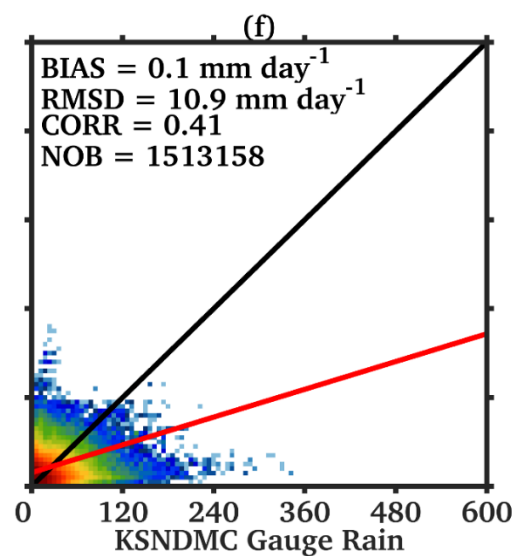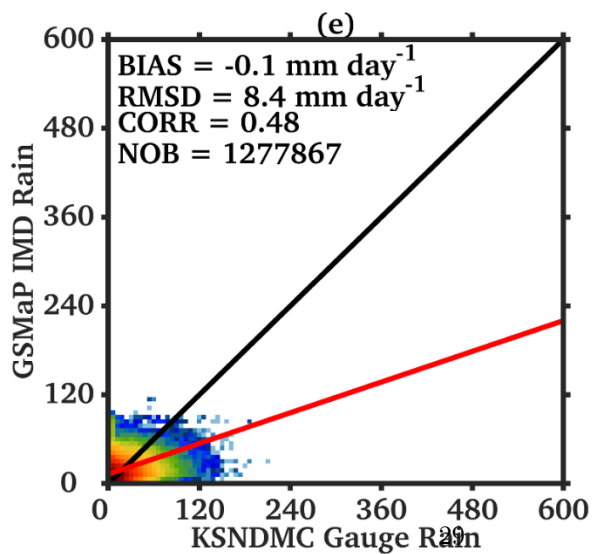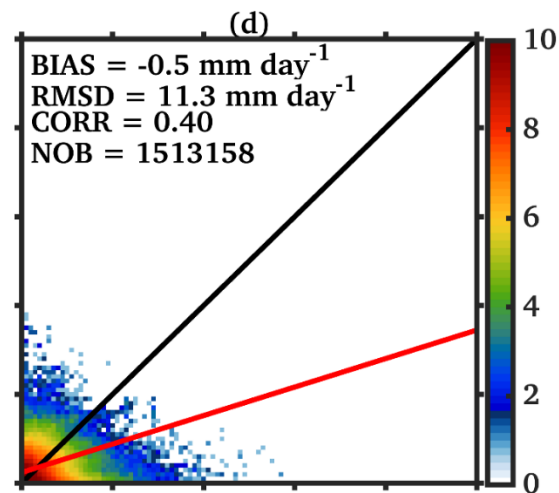
(a)

BIAS = 0.4 mm day^{-1}
RMSD = 8.7 mm day^{-1}
CORR = 0.51
NOB = 1277867

IMERG Final Rain

(b)

BIAS = 1.2 mm day^{-1}
RMSD = 12.4 mm day^{-1}
CORR = 0.44
NOB = 1513158

(c)

BIAS = -0.2 mm day^{-1}
RMSD = 8.5 mm day^{-1}
CORR = 0.50
NOB = 1277867

GSMaP CPC Rain

(d)

BIAS = -0.5 mm day^{-1}
RMSD = 11.3 mm day^{-1}
CORR = 0.40
NOB = 1513158

(e)

BIAS = -0.1 mm day^{-1}
RMSD = 8.4 mm day^{-1}
CORR = 0.48
NOB = 1277867

GSMaP IMD Rain

(f)

BIAS = 0.1 mm day^{-1}
RMSD = 10.9 mm day^{-1}
CORR = 0.41
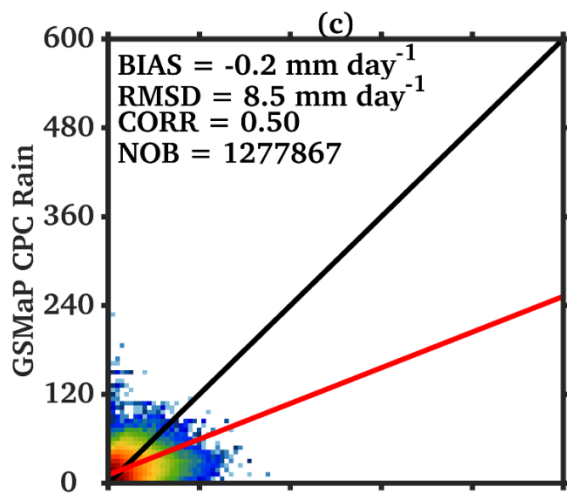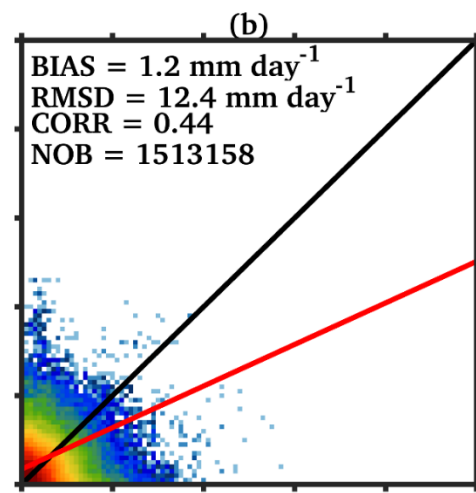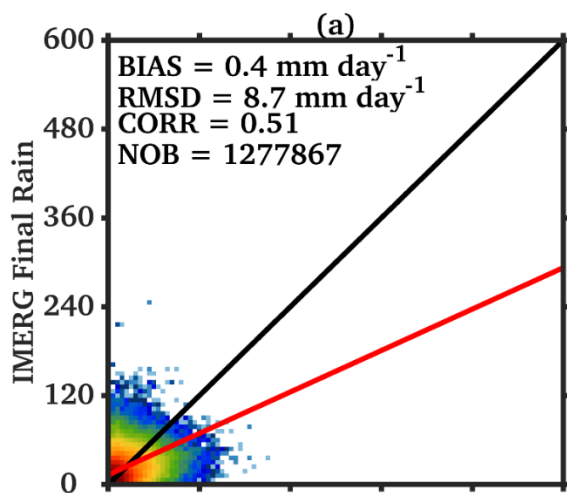NOB = 1513158

KSNDMC Gauge Rain

KSNDMC Gauge Rain

Figure 11. Same as Figure 10, but for (a, c, e) SIK and (b, d, f) NIK regions.